ADVANCED FUNCTIONAL MATERIALS

FULL PAPER

DOI: 10.1002/adfm.200800683

Efficient Polymer Solar Cells with Surface Relief Gratings Fabricated by Simple Soft Lithography**

By *Seok-In Na, Seok-Soon Kim, Jang Jo, Seung-Hwan Oh, Juhwan Kim,* and *Dong-Yu Kim**

Polymer-based photovoltaic cells, with periodic sub-micrometer structures as an efficient light-trapping scheme, are investigated to improve the performance of organic solar cells based on poly(3-hexylthiophene) and 1-(3-methoxycarbonyl)propyl-1-phenyl-(6,6)C_{61}. A soft lithographic approach that uses photoresponsive azo polymer films as masters and poly(dimethylsiloxane) as stamps is used to form surface relief gratings (SRGs) on the active layers. The effect of periodic gratings on solar cell performance is precisely investigated according to various grating conditions such as period, depth, and dimension. The solar cells with 1D and 2D SRGs present improved incident-photon-to-current conversion efficiencies and an overall increase in power conversion efficiencies, primarily resulting from the enhancement of short-circuit current density, indicating that periodic structures induce further photon absorption in the active film.

1. Introduction

Polymer-based bulk-heterojunction (BHJ) solar cells for the fabrication of cost-efficient and flexible power sources have undergone considerable development, including improvements in organic synthesis and fabrication technologies, thus providing a chance to raise the power conversion efficiencies of cells.[1–12] Among the various polymer-based BHJ systems, poly(3-hexylthiophene) (P3HT) and 1-(3-methoxycarbonyl)-propyl-1-phenyl-(6,6)C_{61} (PCBM) networks produced by spin-coating the blends have shown the highest efficiency (4–5%) under 80 or 100 mW cm^{-2} illumination with air mass (AM) 1.5 global (G) conditions; however, further improvement in efficiency is required for commercial applications.[11,12]

Typically, the efficiency of P3HT and PCBM-based organic solar cells (OSCs) is limited because of the weak absorbance of the thin photoactive layer in the range of the solar spectrum. To solve this problem, the thickness of the active layer should be increased to better absorb the impinging photons. However, a thick active layer results in an increase in series resistance of the device as a result of the limited charge-carrier mobility of the conjugated polymers, which ultimately reduces the fill factor (FF).[12] This indicates that a trade-off exists between the absorption of incident light and series resistance, leading to a compromised OSC design and resulting in limited power conversion efficiency of OSCs. Hence, either an exploration of novel device design or the implementation of novel materials to maximize the use of incident light illuminating the solar cell is required.

A promising approach to improve light absorption without increasing photoactive-layer thickness is to trap light in the active layer by using a periodic grating. Periodic structures for light trapping have been used extensively. In particular, this method has been used to enhance optical pass length, thereby increasing the absorption and power conversion efficiency of silicon solar cells.[13–15] However, until very recently, only a few approaches for trapping light in organic-based solar cells or photodiodes have been reported,[16–20] in contrast to the extensive studies on Si solar cells. Most of the work on light trapping within conjugated-polymer-based cells has focused on the simulation and characterization of optical properties rather than power conversion efficiency (η) through current–voltage (I–V) measurements,[16,17] and in some cases, enhanced absorption did not increase the photocurrent generated from the photovoltaic devices.[18] Therefore, to enhance η, practical approaches to light trapping, including development of optimized grating conditions and damage-free polymer patterning processes, are required.

In this study, use of periodic sub-micrometer structures in an efficient light-trapping scheme was investigated for high-performance OSCs based on P3HT and PCBM. The gratings are formed on an active layer by a soft lithographic approach that uses photoinduced surface-relief gratings (SRGs) on azo polymer films[21–23] as masters and poly(dimethylsiloxane) (PDMS) as stamps. Recently, we introduced this approach to

[*] Prof. D.-Y. Kim, S.-I Na, J. Jo, S.-H. Oh, J. Kim
Heeger Center for Advanced Materials
Department of Materials Science and Engineering
Gwangju Institute of Science and Technology
1 Oryong-Dong, Buk-Gu, Gwangju 500-712 (Korea)
E-mail: kimdy@gist.ac.kr
Prof. S.-S. Kim
School of Materials Science and Chemical Engineering
Kunsan National University
Kunsan, Chonbuk, 573-701 (Korea)

[**] This work was financially supported by the Heeger Center for Advanced Materials (HCAM), the Ministry of Education of Korea through the Brain Korea 21 (BK21) program, the Korea Science and Engineering Foundation (KOSEF) through the National Research Lab Program funded by the Korean government (MEST) (M10500000077-06J0000-07710).

ADVANCED FUNCTIONAL MATERIALS

polymer solar cells and showed that the grating made by a soft lithographic technique results in enhanced light trapping in cells.[9] Here, the influence of various grating conditions, such as period, height, and dimension, on solar-cell performance was more precisely investigated based on optical and electrical characterization of the cells.

2. Results and Discussion

The fabrication of P3HT/PCBM-based OSCs with SRGs formed by a soft lithographic approach is presented in Scheme 1. To prepare a master, poly(disperse orange 3) (PDO3) as an azo-functionalized polymer was synthesized from the diglycidyl ether of bisphenol A and disperse orange 3, and then reprecipitated using tetrahydrofuran and methanol.[24] PDO3 films were prepared using 10 wt% PDO3 in cyclohexanone by a spin-coating process followed by drying at 100 °C. 1D and 2D SRGs on PDO3 were formed by exposure to an interference pattern of Ar^+ laser beams (488 nm, 100 mW cm^{-2}). To obtain 2D SRGs, after the formation of 1D SRGs, the substrate was then rotated by 90° around its normal axis followed by a second exposure.[25] To fabricate PDMS molds, the polysiloxane pre-polymer was prepared by mixing the elastomer base and curing agent (Sylgard 184, Dow Corning) in a ratio (10:1, wt/wt). Then the polysiloxane pre-polymer was poured onto the azo masters with SRGs followed by curing at 60 °C. Finally, the PDMS molds were separated from the masters and used for soft contact printing. To fabricate BHJ solar cells with SRGs, poly(3,4-ethylenedioxythiophene):poly(styrenesulfonate) (PEDOT:PSS) was spin-coated onto indium tin oxide (ITO). A solution of P3HT (30 mg) and PCBM (24 mg) in 2 mL of chlorobenzene was then spin-coated on top of the PEDOT:PSS layer, which formed the active layer with a thickness of about 80 nm. To inscribe the SRG pattern on the active layer, the PDMS mold with replicated SRGs from the azo polymer master was put in conformal contact with the active layer. The PDMS mold was kept in nitrogen for 20 min during the annealing process, which was performed at 110 °C to enhance the degree of P3HT ordering.[3] After removal of the PDMS mold, calcium (20 nm) and aluminum (100 nm) were thermally evaporated onto the P3HT/PCBM active layer with SRGs, in a vacuum at 10^{-6} Torr (1 Torr = 133.322 Pa).

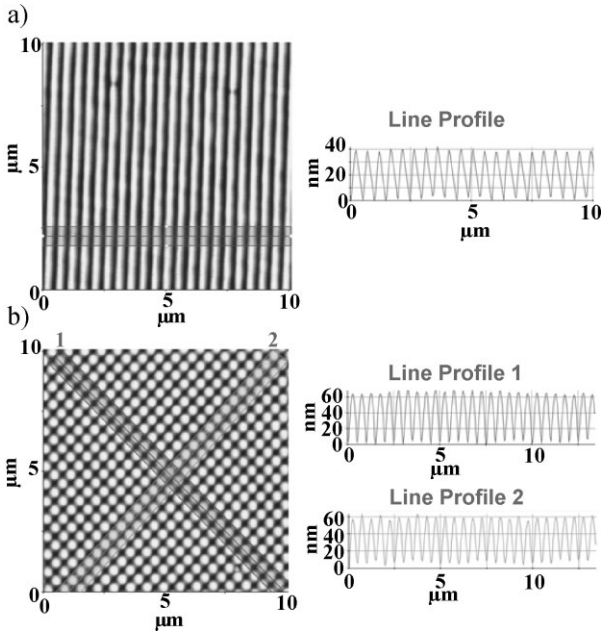

Figure 1. AFM images of a) 1D (period = 500 nm, height = ~40 nm) and b) 2D (period = 500 nm, height = ~60 nm) SRGs on azo polymer films.

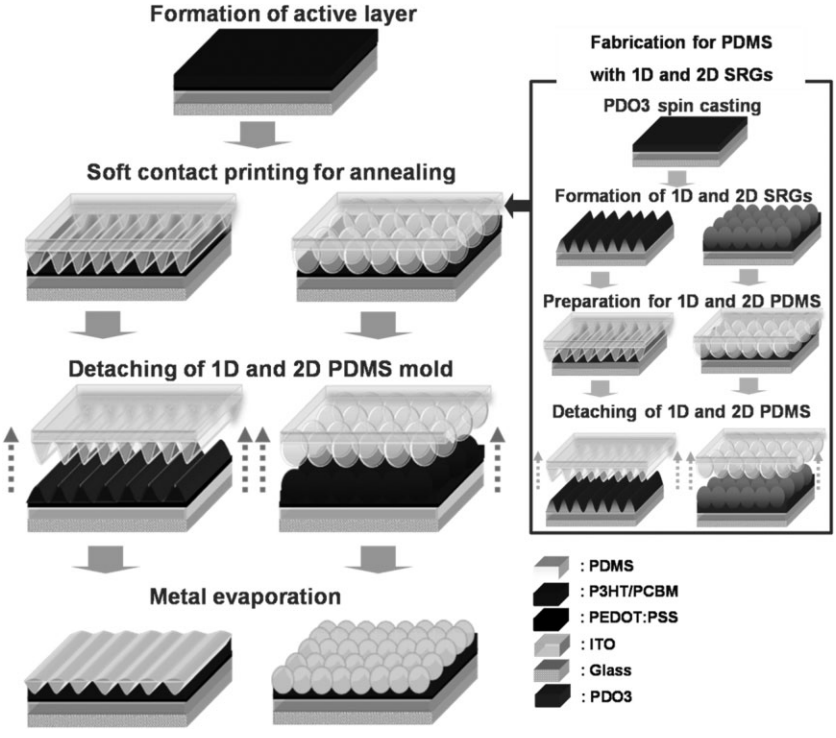

Scheme 1. Schematic representation of the fabrication sequence for bulk-heterojunction solar cells with SRGs formed by a soft lithographic approach.

Preparation of the azo master, having SRGs on the PDO3 azo polymer films, was confirmed by atomic force microscopy (AFM). Using a one-step illumination process and superposition of two sets of gratings with an orthogonal orientation, the 1D (period = 500 nm, height ≈40 nm) pattern and 2D orthogonal cross-grating pattern (period = 500 nm, height ≈60 nm) were obtained on the polymer films, as shown in Figure 1a and b, respectively. Here, the height and period of SRGs can be controlled

by the irradiation time and the incident angle of the interfering Ar^+ laser beams, respectively. Compared to the conventional photolithographic method, the use of azo polymers as a master can provide significant advantages as follows: it is a one-step process; duplication of the method is feasible; it allows control of the grating profiles; it has the capability of superimposing multiple patterns; and, azo polymers are easily prepared.[25–28]

Preparation of the PDMS molds with SRGs was successfully confirmed by AFM, as shown in Figure 2. The 1D (period = 500 nm, height ≈20 nm) and 2D (period = 500 nm, height ≈20 nm) SRGs on the PDMS molds are shown in Figure 2a and b, respectively. PDMS molds replicate the inversed structures of azo masters topologically, as shown in Figures 1 and 2. In addition, the SRGs of PDMS molds have an identical period but a somewhat shallower height than those of the masters. The shallower height of SRGs on PDMS molds is believed to be because the PDMS might not have a surface energy low enough to reproduce small features with a submicrometer size.[23]

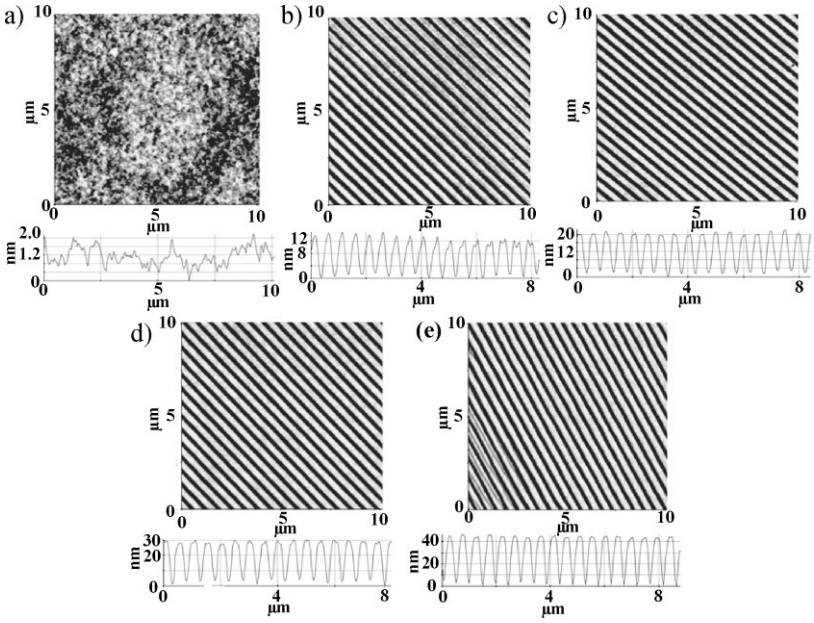

Figure 3. AFM images of the P3HT/PCBM active layers with and without SRGs: a) the active film of the conventional solar cell; b–e) the active layers with SRGs of period 500 nm and varying heights, given respectively approximately as b) 10; c) 20; d) 30; and e) 40 nm (each line profile *y*-axis has units of nm).

The P3HT/PCBM active layers with and without SRGs were confirmed by AFM, as shown in Figure 3. The active layer of the conventional OSC shows typically smooth surfaces with a root mean square (rms) roughness of approximately 0.76 nm, as shown in Figure 3a. Figure 3b–e presents AFM images of the SRGs on the P3HT/PCBM active layer with a grating period of 500 nm and approximate heights of 10, 20, 30, and 40 nm, respectively. It can be confirmed that SRGs on the P3HT/PCBM active layer with the same grating period and height as the PDMS mold were successfully formed by soft contact printing, as shown in Figure 2a and Figure 3c. Interestingly, the PDMS stamp profile was transferred to the polymer film with high fidelity without application of pressure during the soft contact printing. In addition, when the reflective cathodes were evaporated onto the patterned P3HT/PCBM active layer, the period, height, and shape of the reflective cathode were nearly identical to those of the patterned active layer.

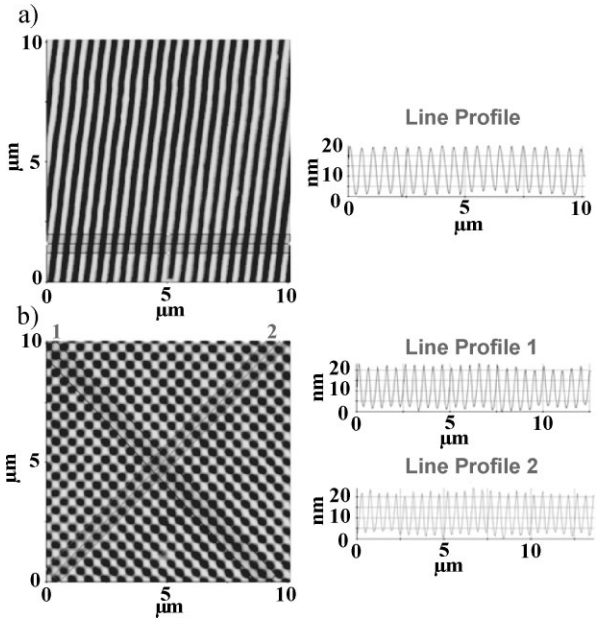

Figure 2. AFM images of a) 1D (period = 500 nm, height = ~20 nm) and b) 2D (period = 500 nm, height = ~20 nm) SRGs on PDMS molds.

A schematic diagram of the organic solar cell structure with SRGs produced by the soft contact printing is shown in Figure 4. As shown in Figure 4, when periodic gratings are provided on the photoactive layer of the organic solar cell, incident light reaching the grating can be diffracted backwards according to the following equation:

$$m\lambda = n_{\text{active}} p(\sin\theta_{\text{i}} + \sin\theta_{\text{d}}) \quad (1)$$

where m is the diffraction order, λ is the wavelength of incident light, n_{active} is the refractive index of the active layer, p is the grating period, and θ_{i} and θ_{d} are the incidence and diffraction angles, respectively. According to Equation 1, for $300\,\text{nm} \le \lambda \le 500\,\text{nm}$ and for $500\,\text{nm} < \lambda \le 700\,\text{nm}$ under normal incidence, m takes values of 0, ±1, and ±2 and values of 0 and ±1, respectively, because of the following

ADVANCED FUNCTIONAL MATERIALS

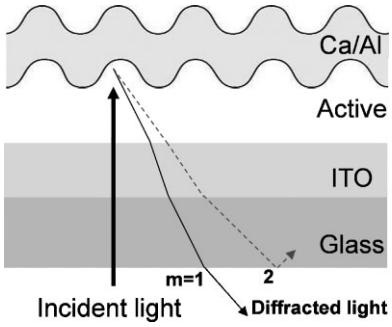

Figure 4. Schematic representation of the structure of an organic solar cell with periodic gratings.

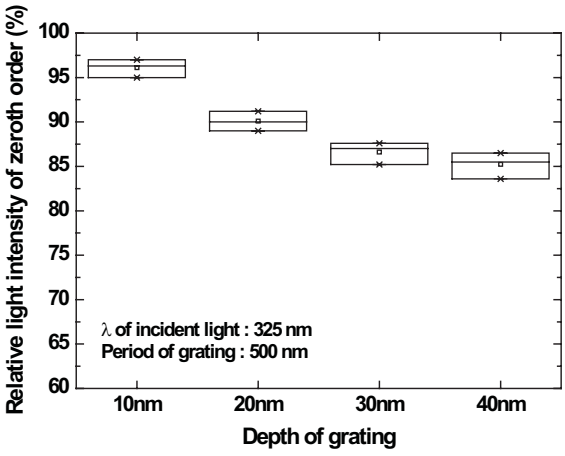

Figure 5. Relative intensity of diffracted light as a function of grating depth (approximate values of 10, 20, 30, and 40 nm) under $\lambda = 325$ nm illumination and 500 nm grating period.

conditions: $\sin\theta_d \leq 1$ and $p = 500$ nm in the present design. Here, to simplify the calculations, a constant n_{active} was considered as 2 in the spectral wavelength range between 300 and 700 nm.[29,30] In fact, because the zeroth order reflection is reduced by periodic gratings, the diffraction at high orders occurs and the diffracted light at high orders can be bent by 90°. For example, as illustrated in Figure 4, when the incidence light ($\lambda = 325$ nm) impinges onto the backside grating, the first- and second-order reflections can be bent by 18.9° and 40.5°, respectively, according to Equation 1. In addition, if $\lambda = 500$ nm, the first- and second-order reflections can be bent by 30° and 90°, respectively. Therefore, the SRGs in OSCs can enhance the optical path length across a broad wavelength range of incident light. Furthermore, if θ_d is greater than the critical angle ($\theta_c = 1/\sin(1/n_{active}) = 30°$) for total internal reflection, induced by applying Snell's law to every interface in a multilayered OSC ($n_{air} = 1$, $n_{glass} \approx 1.5$, $n_{ITO} \approx 2$, $n_{PEDOT} \approx 1.6$, and $n_{active} \approx 2$),[13,29] then total internal reflection will occur at the front surface (air–glass interface) of the OSC and the light can be reflected back to the active film, leading to further absorption.

To quantitatively demonstrate bendable light by SRGs, as shown in Figure 3, relative light intensity of zeroth order as a function of grating depth (with approximate values of 10, 20, 30, and 40 nm) was measured, and the results are shown in Figure 5. Intensity of zeroth order is normalized to the solar cell without a grating. A HeCd laser with $\lambda = 325$ nm was used to illuminate the OSCs with SRGs and the light intensities of zeroth order were measured by a Si photodiode. Figure 5 shows that light intensity of zeroth order was reduced as grating depth increased, indicating that it is possible to bend light by SRGs in cells and achieve higher diffraction intensity at high orders as grating depth increases.

To investigate the effect of grating on the performance of OSCs, solar cells based on P3HT/PCBM with different grating depths were fabricated and compared. Cell performance was measured under 100 mW cm^{-2} illumination from a 1 kW Oriel solar simulator with an AM 1.5 G filter in a N_2-filled glovebox. Figure 6 shows the influence of the grating depth on the power conversion efficiency (η), short-circuit current density (J_{sc}), fill factor (FF), and open-circuit voltage (V_{oc}) of solar cells. Compared with efficiencies of cells without SRGs, the efficiencies of cells with SRGs were all enhanced except for the cell with a grating depth of ~40 nm. The cell with a grating depth of 20 nm showed the maximum value of efficiency, and

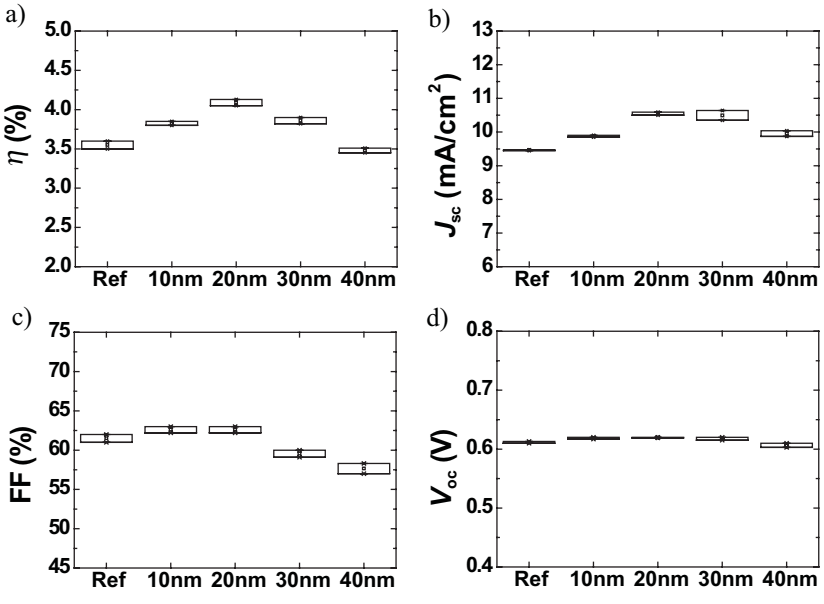

Figure 6. Influence of the grating depth (*x*-axes) on the a) power conversion efficiency (η), b) short-circuit current density (J_{sc}), c) fill factor (FF), and d) open-circuit voltage (V_{oc}) of solar cells.

higher grating depth led to lower efficiency because of a decrease in FF. The decrease of FF in the OSCs with grating depths of 30 and 40 nm means an increase in series resistance (R_s), decrease of shunt resistance (R_{sh}), or both an increase of R_s and decrease of R_{sh}. In fact, compared with the reference cell, the R_s values of the OSCs with grating depths of ~30 and ~40 nm were increased by approximately 15 and 25%, respectively, and the R_{sh} values were decreased by approximately 24 and 40%, respectively. The decrease of FF in cells with grating depths of ~30 and ~40 nm might be attributed to too large a thickness modulation, considering the thickness of the active layer at ~80 nm and the thickness of the Ca layer at ~20 nm, which could induce nonuniform metal contact of the Ca/Al cathode. In cells with SRGs, most of the increase in the cell efficiency comes from the increased J_{sc} through the application of periodic structures rather than FF or V_{oc}, as shown in Figures 6b, c, and d, respectively.

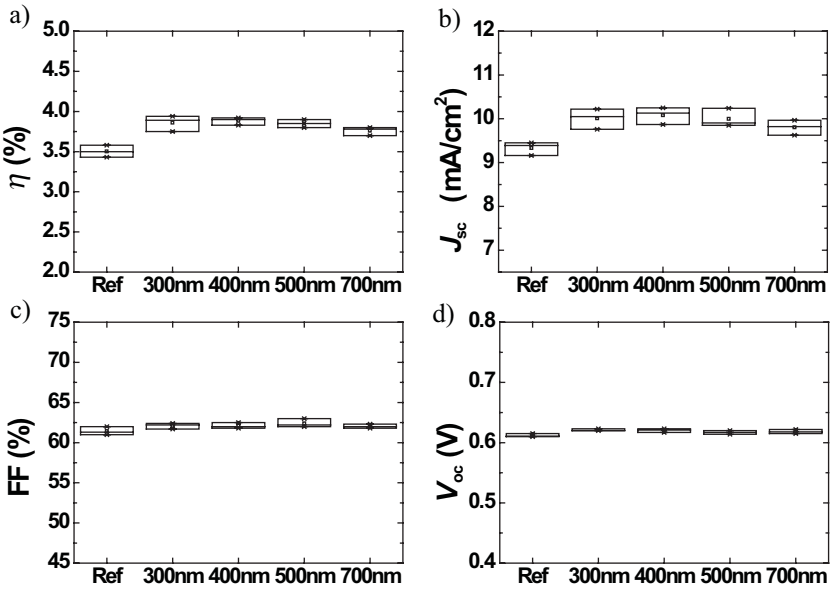

Figure 8. Influence of the grating period (*x*-axes) on the power conversion efficiency (a), short-circuit current density (b), fill factor (c), and open-circuit voltage (d) of solar cells.

Besides the grating depth, the grating period is another important parameter to be optimized for enhancing cell efficiency. The P3HT/PCBM active layers with different grating periods of SRGs were confirmed by AFM. Figure 7 presents AFM images of the SRGs on the P3HT/PCBM active layer with a grating depth of ~10 nm and periods of approximately 300, 400, 500, and 700 nm, respectively. To investigate the effect of the grating period on the performance of OSCs, solar cells based on P3HT/PCBM with different grating periods were fabricated and compared. Figure 8 shows the influence of the grating periods on η, J_{sc}, FF, and V_{oc} of the solar cells. Compared with the reference cell, values of η and J_{sc} for cells with SRGs were all enhanced, and the cell with a grating period of 500 nm showed more enhanced η than that of 700 nm, as expected. However, the overall performances of cells with 300, 400, and 500 nm periods of SRGs were similar to one another. In fact, according to Equation 1, it is expected that the optical path length can be considerably enhanced because a smaller period leads to a larger bending angle of light, resulting in higher cell efficiencies. For example, at $\lambda = 500$ nm, the first-order diffraction angle is 30° for the 500 nm grating period of SRGs and ~56° for the 300 nm grating period of SRGs, indicating SRGs with smaller periods result in larger bending angles of diffracted light. However, the grating equation cannot reflect the amplitude for diffraction orders, and it is found that the diffracted light with a larger bending angle comes with a smaller amplitude, namely a smaller diffraction efficiency; thus, it is believed that OSCs with a smaller grating period do not necessarily show a more enhanced cell efficiency.[31]

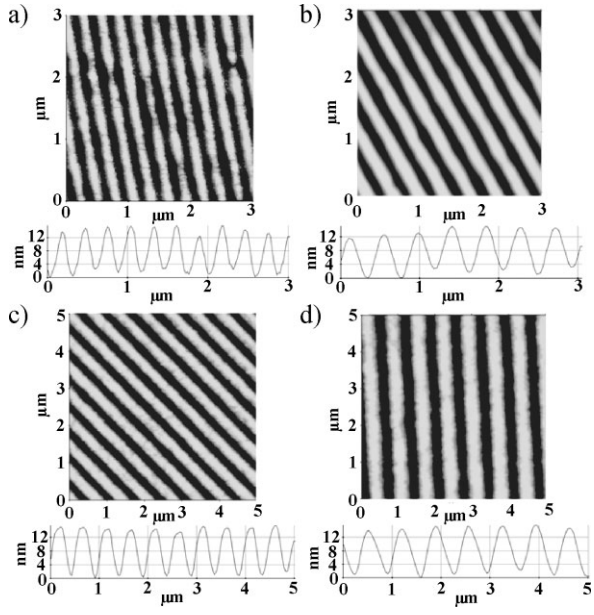

Figure 7. AFM images of the SRGs on the P3HT/PCBM active layer with a grating depth of approximately 10 nm each and a period of approximately a) 300, b) 400, c) 500, and d) 700 nm (each line profile *y*-axis has units of nm).

The P3HT/PCBM active layers with different grating shapes of SRGs were prepared to further enhance cell efficiency. As shown in Figure 9, AFM confirms the P3HT/PCBM active layers and metal cathodes with 1D and 2D SRGs. The 1D (period = 500 nm, height ≈20 nm) and 2D (period = 500 nm, height ≈20 nm) SRGs on the P3HT/PCBM active layers are shown in Figure 9a and c, respectively. Successful formation of 2D SRGs on the P3HT/PCBM active layer with the same grating period and height as the PDMS mold with 2D SRGs

ADVANCED FUNCTIONAL MATERIALS

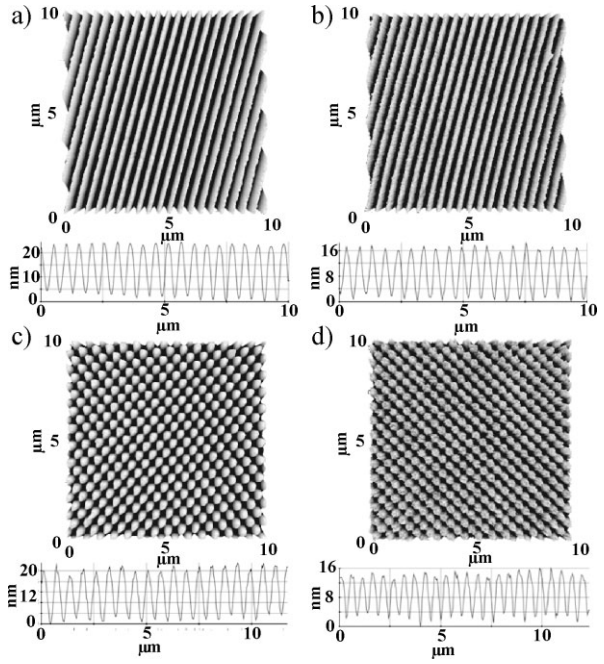

Figure 9. AFM images: a) the active layer with 1D SRGs; b) the reflective cathode evaporated onto the patterned active layer; c) the active layer with 2D SRGs; d) the reflective cathode evaporated onto the active layer with 2D SRGs (each line profile *y*-axis has units of nm).

was confirmed by AFM, as shown by comparing Figures 2b and 9c. In addition, the period, height, and shape of the metal cathodes, which were evaporated onto the patterned active layers, were nearly identical to those of the patterned active layer, as shown in Figure 9b and d.

Figure 10 shows the relative light intensity of zeroth order as a function of wavelength (at $\lambda = 325$, 488, and 632 nm), and the photographic images of Figure 10 show the diffracted light in the reference cell, in the cell with a 1D SRG, and in the cell with a 2D SRG, under conditions of $\lambda = 325$ nm and $p = 500$ nm in each case. HeCd, Ar^+, and HeNe lasers with $\lambda = 325$, 488, and 632 nm, respectively, were used to illuminate the OSCs with SRGs, shown in Figure 9, and light intensities of zeroth order were measured by a Si photodiode. Intensity of zeroth order is normalized to the solar cell without a grating. The results were obtained from the average values measured at three OSCs with 1D and 2D SRGs. From Figure 10, it is clear that light bending was achieved in a broad range, especially interested wavelength at the P3HT/PCBM-based OSCs and that it is possible to achieve stronger diffraction intensity in OSCs with 2D SRGs compared to 1D SRGs.

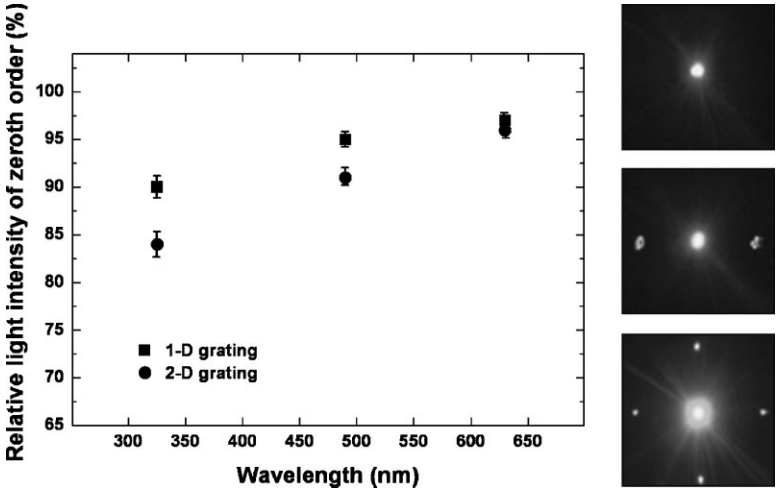

Figure 10. Relative intensity of diffracted light as a function of wavelength. Intensity of diffracted light is normalized to the cell without any grating. Right-hand side images are photographs of diffracted light in the reference cell (top), in the cell with a 1D SRG (middle), and in the cell with a 2D SRG (bottom), when $\lambda = 325$ nm and $p = 500$ nm.

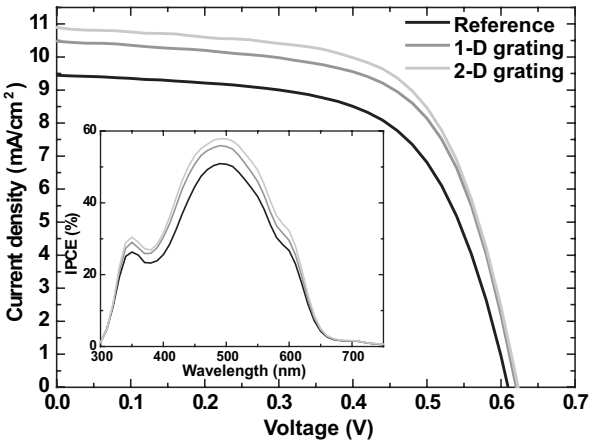

Figure 11. *J–V* characteristics for three kinds of solar cells: a reference cell; a cell with 1D SRGs; and a cell with 2D SRGs. Inset: IPCE spectra for the three cells.

To investigate the effect of 1D and 2D gratings on the performance of OSCs, photocurrent-density–voltage (*J–V*) curves and incident-photon-to-current conversion efficiency (IPCE) were measured and are shown in Figure 11. As demonstrated in this figure, a V_{oc} value of 0.61 V, J_{sc} of 9.5 mA cm^{-2}, FF of 62%, and η of 3.6% were obtained for the reference cell under 1 sun with AM 1.5 G illumination. In contrast, the performance characteristics of the two cells with 1D and 2D SRGs were enhanced as follows: V_{oc} of 0.62 V; J_{sc} of 10.5 and 10.9 mA cm^{-2}; FF of 63 and 64%; and, η of 4.1 and 4.3%, respectively. Compared to the cell with 1D SRGs, an increased efficiency in the cell with 2D SRGs can be attributed to an enhanced diffraction intensity in the broad wavelength range, as shown in Figure 10. From Figure 11, it is clear that most of the increase in cell efficiency originated from the increased J_{sc} through the application of periodic structures rather than V_{oc} or FF, considering that the cell efficiency is proportional to the product $J_{sc}V_{oc}$FF. This observation is in agreement with the IPCE measurement, as shown in the inset of Figure 11. An enhancement over the entire excitation spectral

range was observed for cells with 1D and 2D SRGs. These results indicate that SRGs induce more photogenerated charge carriers by stronger absorption of incident light by the active film, resulting from an increase of optical path length and light trapping.

3. Conclusions

Overall device efficiencies of P3HT/PCBM-based polymer solar cells were increased by use of SRGs as an efficient light-trapping scheme. A soft lithographic approach, consisting of photoresponsive azo polymers as masters and PDMS as stamps, was used to fabricate OSCs with SRGs. The influence of various grating conditions, such as period, depth, and dimension, on solar-cell performance was precisely investigated. Overall power-conversion efficiencies of OSCs with gratings increased primarily as a result of the enhancement of J_{sc}, indicating that SRGs induce further photon absorption in active layers by increasing the optical path length and light trapping. This periodic structure fabricated by simple soft lithography will play an important role in the realization of high-efficiency and low-cost polymer solar cells.

4. Experimental

Device Fabrication: ITO-coated glass (Samsung Corning Co, Ltd., 10 Ω/square) substrates were cleaned with a special detergent followed by ultrasonication in acetone and isopropyl alcohol and then kept at 100 °C for ~30 min. Each substrate was treated with UV/ozone to improve the wettability of PEDOT:PSS. PEDOT:PSS (Baytron P VPAI 4083) was spin-coated using an aqueous solution that had been filtered using a 0.45 μm filter and was subsequently annealed at 120 °C for 20 min, producing a film ~20 nm thick. For the fabrication of photoactive layers composed of interconnected networks of electron donor and acceptor materials, P3HT (Rieke Metals) and PCBM (Nano-C) were dissolved in chlorobenzene to make 30 and 24 mg mL^{-1} solutions, respectively, followed by shaking at room temperatures for ~12 h. The P3HT and PCBM blend was then prepared by mixing the two separated solutions, and subsequent shaking for ~12 h was performed to obtain a homogeneously mixed blend system. Conventional OSCs and OSCs with SRGs were fabricated by spin-coating the blend solution at room temperature and subsequent annealing at 110 °C for 20 min. Fabrication of the devices was completed by thermal evaporation of a Ca/Al (20 nm/100 nm) metal top electrode with an area of 4.34 mm^2 in a vacuum with a pressure of 10^{-6} Torr.

Characterization: The surface images of all films were obtained using an atomic force microscope (Park Systems XE-100), and the thickness of all films was measured using a surface profiler (Kosaka ET-3000i). Linearly polarized HeCd, Ar^+, and HeNe laser beams with $\lambda = 325$, 488, and 632 nm, respectively, were used as light sources for diffraction tests, and light intensities of zeroth order were measured by a Si photodiode. The photocurrent density–voltage (J–V) curves were measured using a Keithley 4200 source measurement unit. Cell performance was measured under 100 mW cm^{-2} illumination intensity generated from a 1 kW Oriel solar simulator with an AM 1.5 G filter in a N_2-filled glovebox. For accurate measurement, light intensity was calibrated using a radiant power meter and a reference silicon solar cell with certification from the National Renewable Energy Laboratory (NREL). IPCE was measured by using a tungsten quartz halogen light source, a monochromator, filters, reflective optics to provide monochromatic light, a mechanical chopper to modulate the light, and a trans-impedance amplifier to provide the test device signal to the digital-signal-processing equipment. A reference silicon photodiode calibrated for spectral response traceable to NIST (National Institute for Standards and Technology) was used for monochromatic power-density calibration.

Received: May 16, 2008
Revised: July 9, 2008
Published online: November 14, 2008

[1] N. S. Sariciftci, L. Smilowitz, A. J. Heeger, F. Wedl, *Science* **1992**, *258*, 1474.
[2] C. J. Brabec, N. S. Sariciftci, J. C. Hummelen, *Adv. Funct. Mater.* **2001**, *11*, 15.
[3] Y. Kim, S. A. Choulis, J. Nelson, D. D. C. Bradley, S. Cook, J. R. Durrant, *Appl. Phys. Lett.* **2005**, *86*, 063 502.
[4] P. Schilinsky, C. Waldauf, C. J. Brabec, *Adv. Funct. Mater.* **2006**, *16*, 1669.
[5] S.-S. Kim, S.-I. Na, J. Jo, G. Tae, D.-Y. Kim, *Adv. Mater.* **2007**, *19*, 4410.
[6] D. Vak, S.-S. Kim, J. Jo, O.-S. Oh, S.-I. Na, J. Kim, D.-Y. Kim, *Appl. Phys. Lett.* **2007**, *91*, 081 102.
[7] M.-S. Kim, J.-S. Kim, J. C. Cho, M. Shtein, L. J. Guo, J. Kim, *Appl. Phys. Lett.* **2007**, *90*, 123 113.
[8] Y. Kim, S. Cook, S. M. Tuladhar, S. A. Choulis, J. Nelson, J. R. Durrant, D. D. C. Bradley, M. Giles, I. Mcculloch, C.-S. Ha, M. Ree, *Nat. Mater.* **2006**, *5*, 197.
[9] S.-I. Na, S.-S. Kim, S.-S. Kwon, J. Jo, J. Kim, T. Lee, D.-Y. Kim, *Appl. Phys. Lett.* **2007**, *91*, 173 509.
[10] K. Kawano, R. Pacios, D. Poplavskyy, J. Nelson, D. D. C. Bradley, J. R. Durrant, *Sol. Energy Mater. Sol. Cells* **2006**, *90*, 3520.
[11] G. Li, V. Shrotriya, J. Huang, Y. Yao, T. Moriarty, K. Emery, Y. Yang, *Nat. Mater.* **2005**, *4*, 864.
[12] J. Y. Kim, S. H. Kim, H.-H. Lee, K. Lee, W. Ma, X. Gong, A. J. Heeger, *Adv. Mater.* **2006**, *18*, 572.
[13] C. Eisele, C. E. Nebel, M. Stutzmann, *J. Appl. Phys.* **2001**, *89*, 7722.
[14] F. Llopis, I. Tobías, *Sol. Energy Mater. Sol. Cells* **2005**, *87*, 481.
[15] L. Zeng, Y. Yi, C. Hong, J. Liu, N. Feng, X. Duan, L. C. Kimerling, B. A. Alamariu, *Appl. Phys. Lett.* **2006**, *89*, 111 111.
[16] L. S. Roman, O. Inganäs, T. Granlund, T. Nyberg, M. Svensson, M. R. Andersson, J. C. Hummelen, *Adv. Mater.* **2000**, *12*, 189.
[17] M. Niggemann, M. Glatthaar, A. Gombert, A. Hinsch, V. Wittwer, *Thin Solid Films* **2004**, *451–452*, 619.
[18] K. Tvingstedt, M. Tormen, L. Businaro, O. Inganäs, *Proc. SPIE* **2006**, *6197*, 61 970C.
[19] S.-B. Rim, S. Zhao, S. R. Scully, M. D. McGehee, P. Peumans, *Appl. Phys. Lett.* **2007**, *91*, 243 501.
[20] C. Cocoyer, L. Rocha, L. Sicot, B. Geffroy, R. de Bettignies, C. Sentein, C. Fiorini-Debuisschert, P. Raimond, *Appl. Phys. Lett.* **2006**, *88*, 133 108.
[21] D. Y. Kim, S. K. Tripathy, L. Li, J. Kumar, *Appl. Phys. Lett.* **1995**, *66*, 1166.
[22] P. Rochon, E. Batalla, A. Natansohn, *Appl. Phys. Lett.* **1995**, *66*, 136.
[23] B. Liu, M. Wang, Y. He, X. Wang, *Langmuir* **2006**, *22*, 7405.
[24] B. K. Mandal, R. J. Jeng, J. Kumar, S. K. Tripathy, *Makromol. Chem, Rapid Commun.* **1991**, *12*, 607.
[25] S.-S. Kim, C. Chun, J.-C. Hong, D.-Y. Kim, *J. Mater. Chem.* **2006**, *16*, 370.
[26] P. S. Ramanujam, N. C. R. Holme, S. Hvilsted, *Appl. Phys. Lett.* **1996**, *68*, 1329.

ADVANCED FUNCTIONAL MATERIALS

[27] M.-J. Kim, J. Kumar, D. Y. Kim, *Adv. Mater.* **2003**, *15*, 2005.
[28] M. Kim, B. Kang, S. Yang, C. Drew, L. A. Samuelson, J. Kumar, *Adv. Mater.* **2006**, *18*, 1622.
[29] A. J. Moulé, J. B. Bonekamp, A. Ruhl, H. Klesper, K. Meerholz, *Proc. SPIE* **2005**, *5938*, 593 808.
[30] F. Monestier, J.-J. Simon, P. Torchio, L. Escoubas, F. Flory, S. Bailly, R. de Bettignies, S. Guillerez, C. Defranoux, *Sol. Energy Mater. Sol. Cells* **2007**, *91*, 405.
[31] N.-N. Feng, J. Michel, L. Zeng, J. Liu, C.-Y. Hong, L. C. Kimerling, X. Duan, *IEEE Trans. Electron Devices* **2007**, *54*, 1926.